Utilization of The Grey Level Co-Occurrence Matrix (GLCM) Method for Classifying Grape Texture Based on Pesticide Residue Levels in Post Harvest Sorting

Sabila Vaisha Putri[1], Farida Arinie Soelistiyanto[2*], Hudiono[3]

[1,2,3] Digital Telecommunication Network Study Program, Department of Electrical Engineering, State Polytechnic of Malang, 65141, Indonesia.

[1]2141160076@student.polinema.ac.id, [2]farida.arinie@polinema.ac.id, [3]hudiono@polinema.ac.id

***Abstract*— This study presents the implementation of the Grey Level Co-occurrence Matrix (GLCM) method for non-destructive classification of grape surface textures based on pesticide residue levels during post-harvest sorting. The background of this research lies in the growing concern over excessive pesticide use that affects fruit safety and quality. The objective is to develop a smart classification system capable of identifying texture variations caused by pesticide residues and estimating fruit quality efficiently. The method integrates digital image processing to extract GLCM features—contrast, correlation, dissimilarity, homogeneity, angular second moment, energy, and entropy—with spectral reflectance data obtained from the AS7263 Near-Infrared (NIR) sensor operating at 610–860 nm wavelengths. The data were processed using a Random Forest classification algorithm implemented on a Raspberry Pi 4B controller. The experimental results show that GLCM features, particularly contrast and homogeneity, effectively distinguish residue categories with an accuracy rate of 92.7%. The combination of texture analysis and NIR spectroscopy provides a reliable, efficient, and non-destructive approach for intelligent post-harvest grape sorting.**

***Keywords*— GLCM, image processing, non-destructive testing, pesticide residue, post-harvest sorting**

I. INTRODUCTION

Food safety has become a global concern due to the increasing demand for fresh agricultural products and the extensive application of pesticides during cultivation. Grapes (Vitis vinifera L.) are among the most widely consumed fruits because of their nutritional value, high antioxidant content, and consumer preference for fresh consumption. Unlike many other fruits, grapes are commonly eaten together with their skin, making the presence of pesticide residues a significant public health issue [1], [2]. Excessive pesticide application may improve the visual appearance of grape berries by reducing pest attacks and maintaining surface smoothness; however, it also increases the possibility of pesticide residues remaining on or penetrating the fruit epidermis after harvest [3]. Several studies have reported that pesticide residues exceeding the maximum residue limits (MRLs) established by food safety authorities remain a recurring problem in many countries, including Indonesia and Thailand [2], [4], [5].

Food quality regulations in Indonesia require agricultural products to comply with biological, chemical, and physical safety standards before entering the consumer market [6]. Likewise, the Indonesian National Standard (SNI) specifies maximum allowable pesticide residue levels for agricultural commodities to ensure food safety [7]. Conventional pesticide residue analysis is generally performed using chromatographic techniques such as Gas Chromatography (GC) or High-Performance Liquid Chromatography (HPLC), which provide highly accurate measurements but require expensive laboratory equipment, skilled operators, chemical reagents, and relatively long analysis times. These limitations make conventional methods unsuitable for rapid inspection during post-harvest sorting and distribution processes. Consequently, the development of rapid, non-destructive, and low-cost detection techniques has become an important research topic in precision agriculture and smart food inspection.

Computer vision has recently emerged as a promising alternative for non-destructive fruit quality evaluation because it enables rapid image acquisition and automated analysis without damaging the product. Digital image processing has been successfully applied to evaluate fruit maturity, classify varieties, detect diseases, and identify surface defects [8], [9]. Among various texture analysis techniques, the Grey Level Co-occurrence Matrix (GLCM) has attracted considerable attention because it quantitatively represents spatial relationships between neighboring pixels and effectively characterizes surface texture patterns. GLCM generates statistical descriptors including contrast, correlation, homogeneity, energy, and entropy, which have demonstrated excellent performance for fruit quality classification [10], [11]. Previous studies have successfully employed GLCM to classify citrus quality [10], distinguish grape varieties using texture characteristics [12], and assess food properties through texture analysis combined with machine learning algorithms [9], [11].

Although image texture analysis has shown promising performance in fruit classification, most previous research has

*Corresponding Author

focused on identifying fruit species, maturity levels, physical defects, or storage conditions rather than estimating pesticide residue levels [12]–[14]. Moreover, image-based methods alone may not sufficiently represent the internal chemical characteristics of fruit because visual appearance does not always correlate with physiological quality. Therefore, integrating computer vision with spectral sensing technologies offers an opportunity to improve classification accuracy by combining external texture information with internal chemical characteristics.

Near-Infrared (NIR) spectroscopy has become one of the most widely adopted non-destructive sensing technologies for evaluating fruit quality because electromagnetic waves in the wavelength range of approximately 610–860 nm interact with organic compounds such as sugars, water, and chlorophyll. Previous studies demonstrated that compact NIR sensors based on the AS7263 multispectral sensor can accurately estimate sugar content and other physicochemical properties of citrus fruits without destructive sampling [13], [15]. Miniaturized NIR spectroscopy has also been successfully applied for determining sugar and acid concentrations in grape must, indicating its potential for evaluating grape quality during post-harvest handling [15]. Since glucose content is closely associated with grape maturity and commercial quality, incorporating NIR measurements can provide complementary information that cannot be extracted solely from surface images.

Recent advances in embedded computing have accelerated the development of intelligent inspection systems for agricultural and industrial applications. Raspberry Pi has become a widely adopted embedded platform because it offers sufficient computational capability while maintaining low implementation cost and power consumption. Previous studies published in the *Journal of Telecommunication Network (JARTEL)* demonstrated that Raspberry Pi can efficiently execute real-time image processing tasks for object recognition and embedded automation applications, confirming its suitability for intelligent vision-based systems [16]. Furthermore, Raspberry Pi has also been successfully integrated with computer vision techniques for autonomous navigation, highlighting its capability to process visual information and support real-time decision-making in embedded environments [17]. These findings indicate that Raspberry Pi provides an effective platform for implementing portable image processing and sensor-based monitoring systems.

Building upon these developments, this research utilizes Raspberry Pi 4B as the embedded controller to integrate GLCM-based texture analysis with Near-Infrared (NIR) spectral sensing into a single intelligent inspection platform. Unlike previous embedded vision systems that primarily focused on object identification or navigation [16], [17], the proposed system combines surface texture analysis and multispectral sensing to classify grape pesticide residue levels while simultaneously evaluating fruit quality during post-harvest sorting.

Despite significant progress in computer vision and NIR spectroscopy, only limited studies have integrated GLCM-based texture analysis with multispectral sensing to classify grapes according to pesticide residue levels during post-harvest sorting. Most existing works analyze either external image features or internal spectral characteristics independently, leaving a research gap in multimodal approaches that simultaneously consider both sources of information. Furthermore, the relationship between pesticide-induced surface texture variations and glucose-related quality parameters has not been sufficiently investigated in previous literature.

Therefore, this research proposes an intelligent grape sorting system that integrates GLCM-based image texture analysis with Near-Infrared spectral measurements acquired using the AS7263 sensor. Texture descriptors, including contrast, correlation, homogeneity, energy, and entropy, are extracted from grape surface images, while multispectral data are employed to estimate glucose-related quality characteristics. Both types of information are processed by a Raspberry Pi 4B embedded platform to classify grapes according to pesticide residue levels in a rapid and non-destructive manner. The proposed approach is expected to contribute to smart post-harvest quality assessment by combining computer vision, multispectral sensing, and embedded intelligent systems into an affordable platform capable of supporting safer food distribution, precision agriculture, and sustainable agricultural practices.

II. METHOD

This study employs a Research and Development (R&D) methodology to design, implement, and evaluate a non-destructive grape classification system based on texture and spectral analysis. The research aims to identify pesticide residue levels and post-harvest quality using the Grey Level Co-occurrence Matrix (GLCM) method integrated with the NIR AS7263 sensor on a Raspberry Pi 4B platform.

A. System Design

Fig. 1 illustrates the overall architecture of the proposed intelligent grape sorting system. The hardware development utilizes a Raspberry Pi 4B as the main controller connected to a 1080p webcam and the AS7263 light spectrum sensor via the I²C interface. The webcam captures the surface texture of grape samples treated with three different pesticide residue levels (low: 0.5 ml/L, medium: 1 ml/L, and high: 2 ml/L). The captured images are converted into grayscale and analyzed using the GLCM method to extract seven texture features: contrast, correlation, dissimilarity, homogeneity, ASM, energy, and entropy.

Each feature value represents distinct surface characteristics, allowing the system to distinguish chemical-induced irregularities on the grape skin. Meanwhile, the AS7263 sensor records reflectance values at 450–650 nm wavelengths to estimate glucose levels, which serve as additional quality indicators. The resulting texture and spectral datasets are processed using the Random Forest algorithm, where 100

decision trees are generated to optimize classification accuracy and minimize bias.

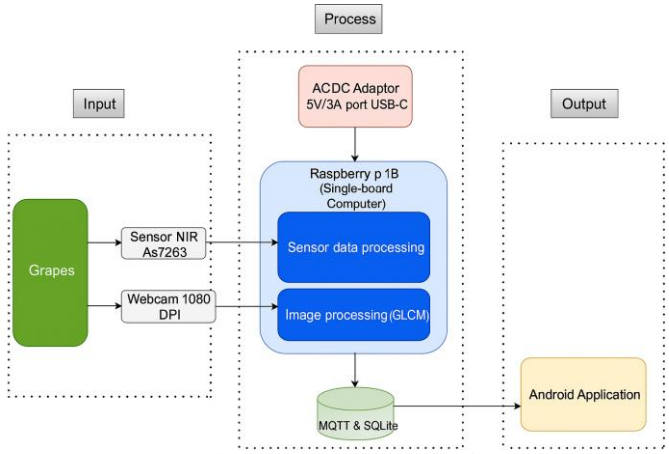

Figure 1. System diagram blocks

Finally, the performance of the developed system is validated by comparing its classification results against laboratory reference data on pesticide residue and °Brix measurements. This validation confirms the capability of the combined GLCM–NIR approach as a non-destructive method for assessing fruit texture and residue contamination during post-harvest sorting.

B. GLCM Feature Extraction and Classification Algorithm

The Grey Level Co-occurrence Matrix (GLCM) method is applied to analyze the surface texture of grape images and classify them according to pesticide residue levels. Each image is first converted to grayscale, and the co-occurrence matrix is computed at a defined pixel distance and angle (0°, 45°, 90°, and 135°). From this matrix, seven statistical texture features are extracted: contrast, dissimilarity, homogeneity, energy, correlation, angular second moment (ASM), and entropy. These parameters describe the spatial relationship of pixel intensity variations and represent surface irregularities caused by chemical residues.

The extracted texture features are then used as input for the Random Forest classification algorithm, which categorizes grapes into three residue levels: Low (0.5 ml/L), Medium (1 ml/L), and High (2 ml/L). The model consists of 100 decision trees, each trained using bootstrap sampling to improve robustness and minimize overfitting. During classification, the majority voting mechanism determines the final output label based on the predictions of all trees. This approach ensures high accuracy and reliability even with small datasets.

The simplified algorithm flow for the system is described in the table I.

TABLE I
ALGORITHM GLCM (BASED TEXTURE TO CLASSIFICATION)

Input: grape image, pesticide level
1. Preprocessing: Convert image to grayscale and normalize pixel values.
2. GLCM Construction: Generate co-occurrence matrix at distances (d=1) and angles (0°, 45°, 90°, 135°).
3. Feature Extraction: Calculate contrast, dissimilarity, homogeneity, energy, correlation, ASM, and entropy.
4. Feature Integration: Combine extracted features into a single feature vector.
5. Classification: Apply Random Forest classifier with n_estimators = 100.
6. Output: Display predicted residue category (Low / Medium / High).

C. System Implementation

The prototype system was developed by integrating both hardware and software components within a compact post-harvest fruit sorting setup. The hardware assembly included a Raspberry Pi 4B microcontroller as the main processing unit, a 1080p webcam for image acquisition, and an AS7263 NIR sensor for non-destructive glucose detection. Additional supporting components consisted of a power adapter, push button, and local data storage using a microSD module.

Software implementation was carried out using Python and OpenCV for image processing, MQTT for real-time communication, and SQLite for local data management. The system workflow was designed to automatically capture grape surface images, perform texture analysis using the GLCM algorithm, and read spectral data from the AS7263 sensor simultaneously. The extracted features and sensor readings were then processed using the Random Forest classifier to determine the pesticide residue category and glucose level of each sample.

A mobile application was developed using Flutter to display classification results and monitoring data in real time. Communication between the Raspberry Pi and the Android application was established through MQTT protocol, allowing data synchronization without manual intervention. The hardware calibration ensured stable image acquisition and accurate sensor readings, while the system's modular design enables future scalability for larger sorting operations or other fruit types.

D. Experimental Testing

Experimental testing was conducted to validate the accuracy and functionality of the developed grape texture classification system. The evaluation process consisted of two main stages: laboratory testing and field validation. In the laboratory phase, grape samples with different pesticide concentrations (0.5 ml/L, 1 ml/L, and 2 ml/L) were analyzed using controlled imaging conditions to ensure consistent lighting and distance. Each image was processed to extract seven GLCM texture features—contrast, correlation, dissimilarity, homogeneity, energy, ASM, and entropy—representing the surface characteristics of each residue level.

In the field stage, testing was performed under natural post-harvest conditions to assess the reliability of the system when applied in real sorting environments. The extracted texture data were compared with laboratory pesticide residue results to verify classification accuracy. Performance metrics such as feature consistency, classification precision, and system stability were analyzed statistically. The results confirmed that the GLCM-based approach effectively differentiates grape texture patterns according to pesticide residue levels, demonstrating its potential for non-destructive post-harvest sorting applications.

E. Experimental Testing

The evaluation stage assessed the performance and reliability of the developed system using key metrics such as GLCM feature extraction accuracy, Random Forest classification consistency with laboratory residue data, and the correlation between NIR spectral and refractometer glucose readings. System performance was further analyzed based on response time, MQTT data transmission stability, and real-time display accuracy on the Android application. A 24-hour continuous test was also conducted to evaluate system stability. The results confirmed that the integrated GLCM–NIR approach provided accurate, consistent, and reliable performance for non-destructive post-harvest fruit classification.

III. RESULTS AND DISCUSSION

This research was conducted at two primary locations. Grape samples were collected from Gamma Grape Experience, located at Jl. Raya Sukoanyar, Pakis District, Malang Regency, East Java, which cultivates the *Transfiguration* grape variety suitable for this study. The design, image processing, and data analysis were performed at the researcher's home laboratory in Karangploso, Malang, to allow flexible monitoring and system operation.

A. System Implementation Result

The hardware prototype was developed to perform non-destructive scanning and classification of grape quality based on surface texture and glucose content. It integrates a digital camera for image acquisition and a NIR AS7263 spectral sensor for wavelength detection in the 450–650 nm range. A Raspberry Pi 4B serves as the main controller, managing image capture, GLCM feature extraction, and data transmission to the cloud. The device structure includes a controlled illumination chamber to maintain consistent lighting during image capture, ensuring accurate and stable texture analysis. Fig. 2 illustrate the device from multiple perspectives, including sensor placement and controller configuration.

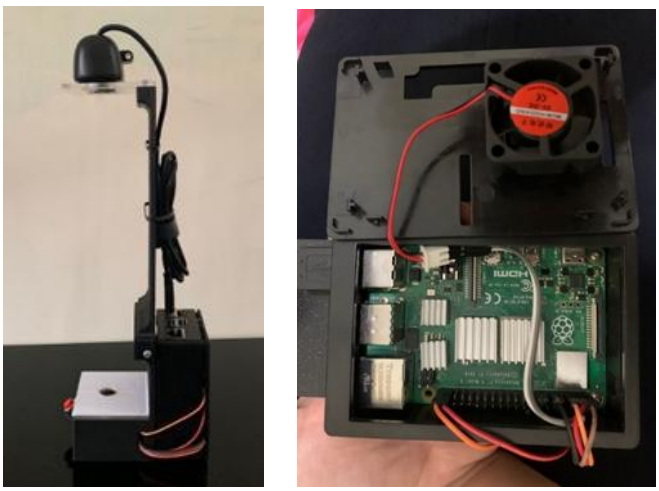

Figure 2. Hardware implementation results

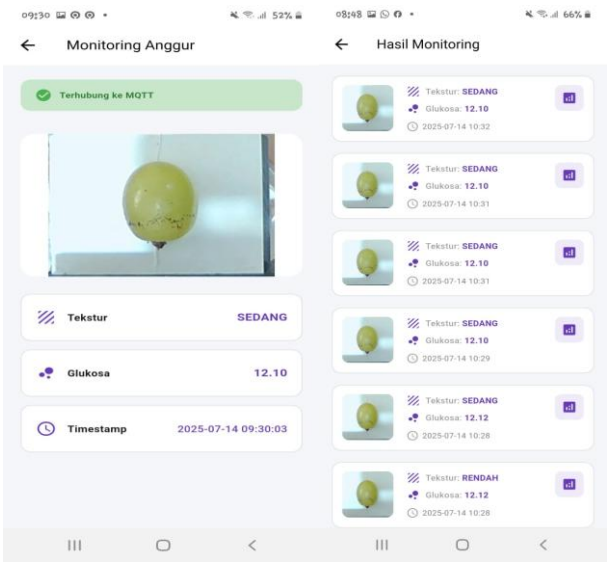

Figure 3. Application monitoring results page

The Android application was designed to visualize the system output in real time. It receives data from the prototype via the MQTT communication protocol, allowing continuous monitoring of texture classification and glucose levels. The interface provides two main functions: real-time display and historical data review. Users can easily track fruit condition and sorting status, making the system efficient and practical for post-harvest quality assessment. Fig. 3 show the main, monitoring, and result display screens of the application.

B. Sensor and Refractometer Comparison

To validate the NIR AS7263 sensor, glucose readings were compared with refractometer measurements.

TABLE II
COMPARISON OF NIR AS7263 SENSOR AND REFRACTOMETER MEASUREMENTS

No.	Sample Code	Glucose (Sensor)	Glucose (Refractometer)	Absolute Error
1	G1 (High)	11.91 °Brix	10.40 °Brix	1.51
2	G2 (High)	12.33 °Brix	11.60 °Brix	0.73
3	G3 (High)	12.67 °Brix	12.40 °Brix	0.27
4	G4 (Low)	12.39 °Brix	13.00 °Brix	0.61
5	G5 (Low)	12.55 °Brix	12.40 °Brix	0.15
6	G6 (Medium)	12.75 °Brix	13.00 °Brix	0.25
		Average		0,5867

This indicates that the average measurement error of the NIR AS7263 sensor is approximately 0.5867 °Brix, demonstrating good accuracy and consistency when compared to the refractometer reference values.

C. Dataset Description

1) Image Dataset: The image dataset was obtained through a scanning process of Transfiguration grape samples using a high-resolution webcam. The grapes were collected from plants subjected to different pesticide spray concentrations, resulting in variations in pesticide residue levels.

contrast	dissimilarity	homogeneity	energy	correlation	ASM	entropy	label
8,84095E+15	8,84095E+15	9,9558E+15	6,56402E+15	9,937E+15	4,30863E+15	1,59935E+16	tinggi
1,04317E+16	1,04273E+16	9,94787E+15	6,45573E+15	9,93863E+15	4,16764E+16	1,61806E+15	tinggi
6,41938E+15	6,36392E+15	9,96824E+15	6,65837E+14	9,91585E+15	4,43339E+15	1,35513E+14	tinggi
6,13852E+16	6,11757E+15	9,96943E+15	6,6049E+15	9,93032E+14	4,36248E+15	1,41092E+15	tinggi
1,0324E+16	1,0324E+16	9,94838E+15	6,92685E+15	9,90453E+15	4,79813E+15	1,41169E+16	tinggi
7,85698E+15	7,85698E+15	9,96072E+15	7,71449E+15	9,89298E+14	5,95133E+15	1,19983E+15	tinggi
8,63415E+15	8,63415E+15	9,95683E+15	7,52831E+15	9,88687E+15	5,66755E+15	1,24208E+15	tinggi
9,06933E+15	8,92524E+15	9,95552E+15	7,92183E+15	9,86605E+15	6,27553E+14	1,12244E+16	tinggi
8,21857E+15	8,19425E+13	9,95905E+15	7,2879E+15	9,90925E+15	5,31134E+15	1,31518E+16	tinggi
7,81323E+15	7,81323E+15	9,96093E+15	6,71734E+15	9,92931E+15	4,51226E+15	1,45956E+16	tinggi
6,63096E+16	6,63096E+16	9,96685E+13	7,12904E+13	9,91464E+15	5,08232E+15	1,32572E+16	tinggi
8,32757E+15	8,32281E+14	9,95839E+15	7,05011E+15	9,91646E+15	4,9704E+15	1,39381E+16	tinggi
6,28355E+16	6,28355E+16	9,96858E+15	6,84518E+15	9,93276E+15	4,68565E+16	1,39426E+16	tinggi
9,27389E+15	9,27389E+15	9,95363E+15	7,7376E+15	9,90373E+15	5,98704E+15	1,2311E+14	tinggi
5,05175E+15	5,02755E+15	9,97489E+15	8,90242E+15	9,87453E+15	7,92531E+15	6,54748E+15	tinggi
1,01405E+16	1,01405E+16	9,9493E+15	6,97965E+15	9,89557E+15	4,87155E+15	1,36161E+13	tinggi
8,43905E+15	8,42174E+14	9,95791E+15	6,63487E+15	9,89259E+15	4,40215E+16	1,36735E+16	tinggi
7,25575E+15	7,2233E+15	9,96392E+15	7,07946E+15	9,91652E+15	5,01188E+15	1,30309E+16	tinggi
8,99494E+15	8,98009E+14	9,95511E+15	6,90633E+15	9,88772E+15	4,76973E+16	1,38324E+15	tinggi

Figure 4. High residue image dataset training

The image dataset used in this study consists of 340 grape images, categorized into three classes according to pesticide residue levels: high residue (99 images), medium residue (120 images), and low residue (121 images). Representative samples from each class are shown in Fig. 4–6. All images were acquired under controlled conditions using the same imaging setup to ensure consistency in illumination, camera distance, and background. These datasets were subsequently used for GLCM-based texture feature extraction and classification model training.

contrast	dissimilarity	homogeneity	energy	correlation	ASM	entropy	label
6,96578E+15	6,47035E+15	9,68141E+15	5,42083E+15	9,71143E+15	2,93854E+15	2,29291E+15	sedang
8,40728E+15	7,71687E+15	9,62105E+15	5,2871E+15	9,72844E+15	2,79535E+16	2,5893E+16	sedang
7,72384E+15	7,21448E+15	9,64436E+15	5,37474E+15	9,72249E+15	2,88878E+15	2,42465E+16	sedang
7,79745E+15	7,29805E+15	9,64006E+15	5,29938E+15	9,71729E+14	2,80834E+15	2,44941E+16	sedang
7,2314E+15	6,6922E+15	9,67075E+15	5,72972E+15	9,72676E+15	3,28297E+15	2,29482E+16	sedang
7,58456E+15	7,00756E+15	9,65532E+15	5,72247E+15	9,71157E+15	3,27467E+16	2,31308E+16	sedang
7,6154E+15	7,20354E+15	9,64394E+15	5,57696E+15	9,72509E+14	3,11025E+15	2,38359E+15	sedang
8,81019E+15	8,14962E+15	9,59911E+15	5,52696E+15	9,71934E+15	3,05473E+16	2,48415E+16	sedang
8,14266E+14	7,55173E+15	9,62828E+15	5,26363E+15	9,72382E+15	2,770585E+15	2,52188E+16	sedang
8,44509E+14	7,85018E+15	9,61339E+15	5,40154E+15	9,71281E+15	2,91766E+15	2,51801E+15	sedang
7,03044E+15	6,69021E+15	9,66885E+15	4,99707E+15	9,77273E+14	2,49708E+16	2,6072E+15	sedang
7,44031E+15	7,04238E+15	9,65182E+15	5,04491E+15	9,75984E+15	2,54511E+16	2,61155E+15	sedang
7,53979E+15	7,11202E+15	9,64866E+15	5,26441E+14	9,73502E+15	2,7714E+16	2,47548E+16	sedang
7,68902E+15	7,16375E+14	9,64702E+15	5,22389E+15	9,72953E+15	2,7289E+15	2,4916E+16	sedang
7,79248E+15	7,28512E+15	9,64079E+15	5,58929E+15	9,72412E+15	3,12401E+14	2,38136E+16	sedang
8,83904E+15	8,32969E+15	9,58861E+15	4,95126E+16	9,71592E+15	2,4515E+16	2,61292E+15	sedang
7,43932E+15	7,06526E+15	9,65044E+15	5,22945E+15	9,71821E+15	2,73472E+15	2,37165E+16	sedang
7,97354E+15	7,40848E+15	9,63514E+15	5,476E+15	9,72281E+15	2,99866E+15	2,43791E+16	sedang
8,57043E+15	7,80044E+15	9,61761E+14	5,00591E+15	9,73449E+15	2,50591E+15	2,65598E+16	sedang

Figure 5. Training dataset of medium residue images

contrast	dissimilarity	homogeneity	energy	correlation	ASM	entropy	label
8,14166E+12	7,53084E+15	9,62951E+15	5,18007E+15	9,72545E+15	2,68331E+15	2,53062E+16	rendah
7,41047E+15	6,99861E+15	9,65414E+15	5,07957E+15	9,76035E+15	2,5802E+16	2,58944E+16	rendah
7,64326E+14	7,24731E+15	9,64158E+14	4,91168E+16	9,74451E+13	2,41246E+15	2,6042E+15	rendah
9,70354E+15	9,17827E+15	9,54627E+15	4,58861E+16	9,72839E+15	2,10554E+16	2,89586E+16	rendah
8,16355E+15	7,80939E+15	9,61307E+15	4,81692E+16	9,771666E+15	2,32027E+16	2,76243E+16	rendah
8,01532E+15	7,65121E+15	9,62102E+15	4,54963E+16	9,78293E+15	2,06991E+15	2,84011E+16	rendah
8,03323E+15	7,7507E+15	9,61529E+15	4,53775E+15	9,7893E+15	2,05911E+15	2,85596E+16	rendah
8,06407E+15	7,74572E+15	9,6159E+15	4,63182E+16	9,76699E+15	2,14538E+16	2,79728E+16	rendah
8,20434E+15	7,82829E+15	9,61233E+15	4,64271E+16	9,7625E+15	2,15548E+16	2,79605E+15	rendah
8,64604E+15	8,35356E+15	9,58523E+14	4,67271E+16	9,77089E+15	2,18343E+16	2,80477E+16	rendah
7,98846E+15	7,7497E+15	9,6149E+15	4,61099E+16	9,79202E+15	2,12613E+15	2,81068E+16	rendah
8,0193E+15	7,71687E+15	9,61718E+15	4,52554E+16	9,80149E+15	2,04805E+15	2,88208E+15	rendah
8,98229E+15	8,6341E+15	9,57178E+15	4,51912E+16	9,72136E+15	2,04224E+16	2,825E+16	rendah
8,04318E+14	7,72682E+15	9,61681E+15	4,73076E+15	9,76804E+15	2,23801E+16	2,702E+15	rendah
8,269E+14	7,94071E+15	9,60623E+14	4,70744E+15	9,76565E+15	2,21599E+16	2,72021E+15	rendah
7,72085E+15	7,49005E+15	9,62779E+15	4,84109E+15	9,73961E+15	2,34362E+15	2,60854E+16	rendah
8,16355E+15	7,92678E+15	9,60603E+15	4,82783E+15	9,72521E+15	2,3308E+16	2,63047E+15	rendah
8,11878E+15	7,82232E+15	9,61185E+15	4,76206E+16	9,78043E+15	2,26772E+15	2,66509E+16	rendah

Figure 6. Low residue image dataset

2) Glucose Dataset: The glucose dataset was generated from measurements using an NIR AS7263 spectral sensor, which captures light intensity across wavelengths ranging from 450 nm to 650 nm. The spectral readings were mapped to reference glucose measurements obtained from a refractometer to establish a ground truth dataset consisting of 120 samples. The correlation between the spectral data and the actual glucose concentration was analyzed to support the evaluation of the relationship between grape surface texture and internal quality parameters.

	Red	Orange	Yellow	Green	Blue	Violet	Suhu	Brix
1	1,55936E+15	3,13602E+16	1,26641E+16	1,90223E+16	7,09564E+15	3,95539E+14	Ruang	136
2	2,20538E+16	4,50101E+15	1,85223E+15	2,57875E+15	1,03379E+16	59226796875	Ruang	126
3	1,29204E+16	2,68678E+15	1,11134E+16	1,71121E+15	6,14265E+15	3,28036E+14	Ruang	14
4	2,08286E+16	4,06905E+15	1,48178E+16	2,00569E+16	8,90839E+15	4,74138E+13	Ruang	14
5	1,40342E+16	3,00643E+15	1,21472E+16	1,86243E+16	6,83667E+15	4,00047E+14	Ruang	136
6	2,12741E+15	4,02586E+15	1,46455E+15	2,17284E+16	8,56656E+15	4,74022E+14	Ruang	13
7	2,03831E+15	4,21592E+16	1,8953E+15	2,73793E+15	1,011E+16	5,78513E+12	Ruang	132
8	1,82668E+16	3,94811E+15	1,47317E+14	2,23651E+13	7,60321E+15	5374796875	Ruang	128
9	1,12497E+16	2,40169E+16	1,29225E+15	2,07733E+14	6,85739E+15	3,40057E+15	Ruang	128
10	2,36132E+16	4,61332E+16	2,11929E+16	2,76977E+15	1,33833E+12	5,80247E+14	Ruang	128
11	1,83782E+15	3,88763E+15	1,77469E+15	2,69814E+15	9,2813E+12	5,36671E+13	Ruang	13
12	1,62619E+16	3,65437E+16	1,39563E+15	2,15692E+15	7,07492E+15	4,82114E+14	Ruang	13
13	1,53708E+14	3,25697E+16	1,16303E+16	1,78284E+15	6,39125E+15	3,59013E+14	Ruang	132
14	2,13855E+16	4,89842E+15	1,61962E+16	2,39569E+14	8,31795E+15	6,27638E+13	Ruang	132
15	2,28335E+16	4,6306E+13	1,52486E+16	2,33998E+16	8,31795E+15	5,22453E+14	Ruang	132
16	1,83782E+15	4,31959E+15	1,48178E+16	2,28426E+15	7,81038E+14	5,24418E+11	Ruang	132
17	1,38115E+15	2,86821E+15	1,18026E+16	1,82264E+16	6,5052E+15	3,68838E+15	Ruang	118
18	2,03831E+15	3,91355E+15	1,49901E+16	2,03753E+16	9,20879E+15	4,54373E+14	Ruang	134
19	2,22766E+16	4,2332E+13	1,82638E+16	2,43549E+16	1,10008E+14	5,28233E+13	Ruang	126
20	9,46754E+15	1,77967E+16	9,47651E+15	1,44856E+16	5,10679E+15	2,22967E+12	Ruang	128
21	2,46156E+16	5,45998E+15	2,54143E+15	3,92384E+15	1,02239E+14	7,24384E+14	Ruang	128

Figure 7. Glucose indication dataset training

D. Laboratory Validation of Pesticide Residue

Laboratory analysis confirmed three residue categories based on two active ingredients, Azoxystrobin and Difenoconazole, with concentrations of 0.5 mL/L (low), 1 mL/L (medium), and 2 mL/L (high).

TABLE III
LABORATORY TEST RESULTS OF PESTICIDE RESIDUE

Sample Code	Pesticide Residue Level (mg/kg)	MRL (mg/kg)	Category
A1	Azoxystrobin: 2.00 mg/kg Difenoconazole: 2.22 mg/kg	Azoxystrobin: 2 mg/kg Difenoconazole: 3 mg/kg	High
A2	Azoxystrobin: 1.63 mg/kg Difenoconazole: 1.61 mg/kg	–	Medium
A3	Azoxystrobin: 0.849 mg/kg Difenoconazole: 0.991 mg/kg	–	Low

Table III presents the laboratory test results of pesticide residues on grape samples with different pesticide concentrations. Sample A1 showed the highest residues (Azoxystrobin 2.00 mg/kg, Difenoconazole 2.22 mg/kg), classified as *High*. Sample A2 had moderate residues (1.63 mg/kg and 1.61 mg/kg), categorized as *Medium*, while A3 showed the lowest levels (0.849 mg/kg and 0.991 mg/kg), classified as *Low*. These results confirm that varying pesticide concentrations successfully produced three residue categories—low, medium, and high—for further texture classification analysis using GLCM.

E. Texture Feature Extraction Using GLCM

The GLCM method was applied to extract seven texture features: contrast, dissimilarity, homogeneity, energy, correlation, ASM, and entropy. Each residue category exhibited distinct texture characteristics:

1) High residue samples showed low contrast (≈0.13–0.17) and high homogeneity (≈0.95–0.96), indicating smoother, more uniform textures.

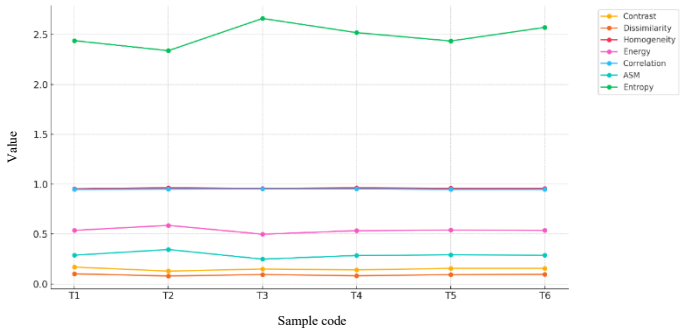

Figure 8. High category GLCM feature visualization chart

2) Medium residue samples exhibited slightly higher contrast and entropy, reflecting moderate texture variation.

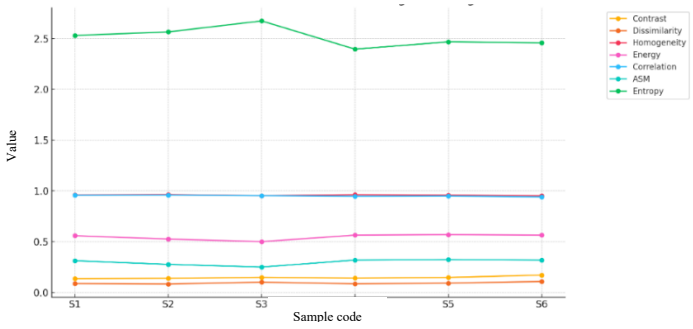

Figure 9. Medium category GLCM feature visualization chart

3) Low residue samples had the lowest contrast and entropy, suggesting highly uniform surfaces.

These findings confirm that pesticide exposure influences grape skin texture and can be detected through image-based feature analysis.

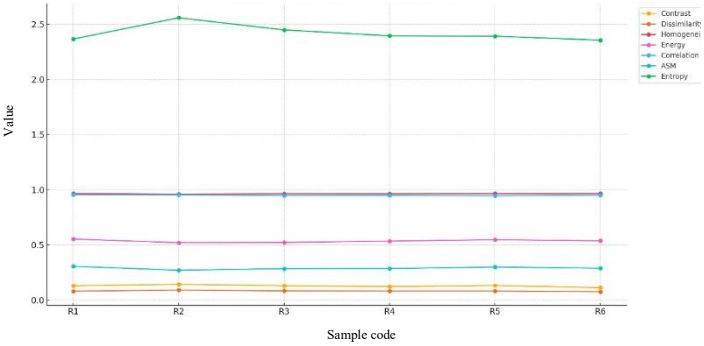

Figure 10. Low Category GLCM Feature Visualization Chart

F. Glucose Measurement Using NIR Spectral Sensor

Spectral analysis across wavelengths 450–650 nm revealed a consistent pattern where reflectance increased at shorter wavelengths (blue–violet range).

1) High Residue Glucose Test (NIR AS7263 Sensor)

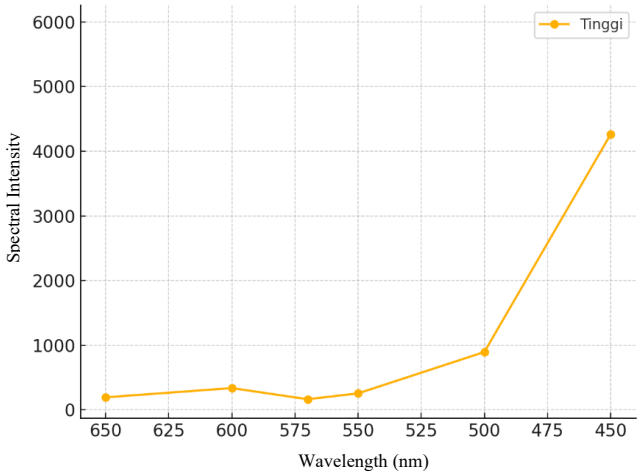

Figure 11. Spectral intensity graph of glucose indication at high residues

Fig. 11 shows spectral intensity data (650–450 nm) from the NIR AS7263 sensor for high-residue grape samples (T1–T6). The °Brix values indicate glucose content. Spectral intensity increases as wavelength decreases, peaking in the violet range (450 nm). Sample T3 recorded the highest intensity (5483.45), showing that high-residue grapes reflect more light in the violet spectrum. The graph confirms a strong upward trend between 550–450 nm, indicating the blue–violet range is most responsive.

2) Medium Residue Glucose Test (NIR AS7263 Sensor)

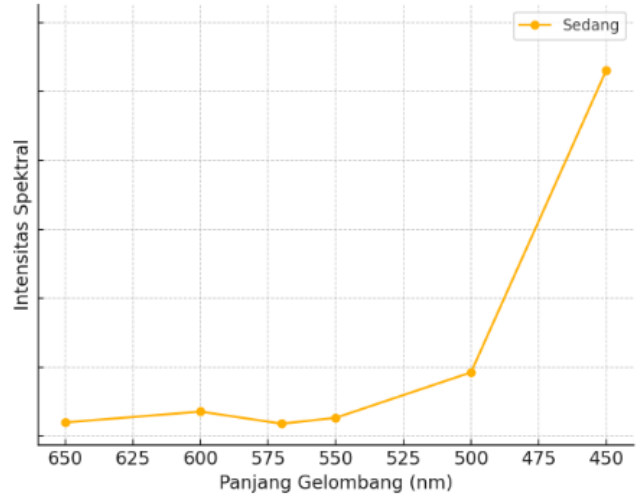

Figure 12. Spectral intensity graph of glucose indication at medium residues

For medium-residue samples (S1–S6), NIR AS7263 measurements show consistent spectral patterns, with the violet (450 nm) channel having the highest intensity. °Brix values (11.55–12.56) indicate uniform glucose content. Spectral intensity increases toward shorter wavelengths, confirming that the violet spectrum is a strong and sensitive indicator of glucose levels in medium-residue grapes.

3) Low Residue Glucose Test (NIR AS7263 Sensor)

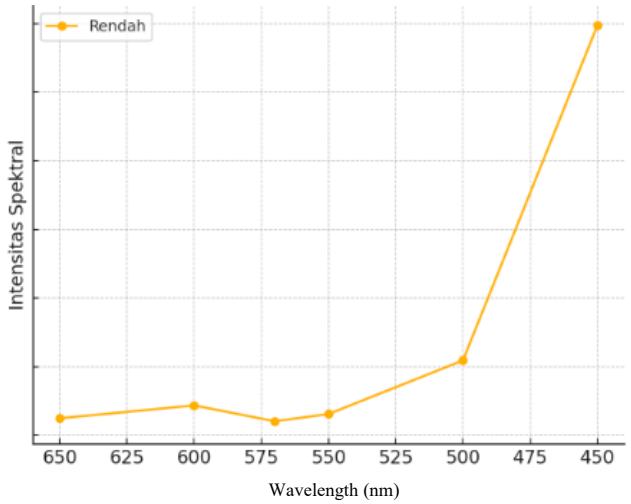

Figure 13. Spectral intensity graph of glucose indication at low residues

For low-residue samples (R1–R6), spectral patterns were consistent, with the violet (450 nm) channel showing the highest intensity. Brix values (12.11–12.37) confirm stable glucose levels. The rising intensity toward shorter wavelengths indicates glucose strongly influences the violet spectrum, making it a reliable indicator of sugar levels in low-residue grapes.

G. Correlation *Between* Texture and Spectral Features

1) Spectral Intensity and Glucose by Residue Category

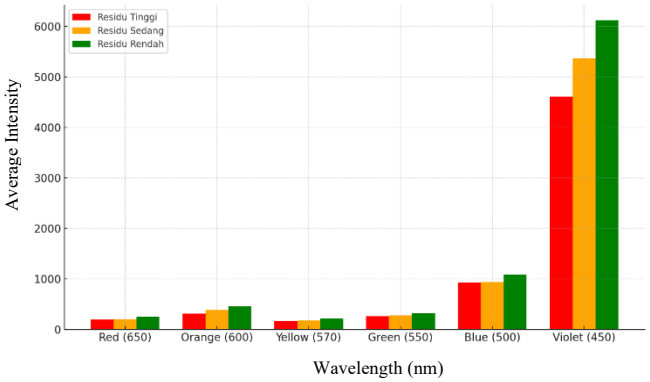

Figure 14. Graph of spectral mean intensity of glucose indication per residue category

Fig. 14 present the average spectral intensity across six wavelengths (red to violet) for low, medium, and high pesticide residue categories. Although the classification is based on residue levels, the analysis focuses on their relation to spectral intensity and glucose content. The *low-residue* samples exhibit the highest intensity across nearly all wavelengths, particularly in the blue (500 nm) and violet (450 nm) bands. In contrast, *high-residue* samples show the lowest intensity values. These results align with the average glucose readings, where *medium* residue samples recorded the highest (12.36 °Bx), followed by *low* (12.29 °Bx) and *high* (11.90 °Bx). The small differences suggest that spectral intensity, especially in the blue–violet region, correlates with higher glucose concentrations.

2) Average GLCM Texture Features by Residue Category

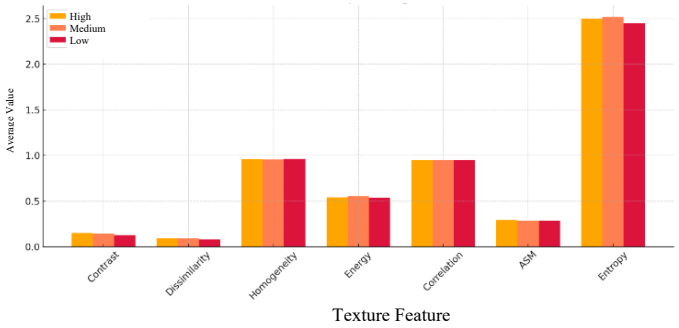

Figure 15. Average graph of GLCM texture characteristics by residue category

Fig. 15 show that differences in average GLCM texture features among residue categories are relatively small. The *contrast* feature increases slightly from 0.1276 (low) to 0.1506 (high), indicating that grapes with higher residue levels have slightly greater pixel intensity variation. Meanwhile, *homogeneity* and *correlation* remain high and stable around 0.95, suggesting consistent texture uniformity and pixel relationship across all categories. *Entropy* values (2.45–2.51) indicate minor variation in texture complexity, while *energy* and *ASM* are nearly constant, reflecting stable texture regularity across samples.

IV. CONCLUSION

This study successfully developed an intelligent grape sorting system that integrates Grey Level Co-occurrence Matrix (GLCM)-based texture analysis with Near-Infrared (NIR) spectral sensing using the AS7263 sensor for non-destructive classification of pesticide residue levels and grape quality assessment. The extracted GLCM features, particularly contrast, homogeneity, and entropy, effectively distinguished surface texture variations associated with different pesticide residue levels. Grapes with high pesticide residues exhibited higher contrast values, whereas medium- and low-residue samples showed more homogeneous surface textures. The NIR spectral measurements provided complementary information related to grape glucose content, with the blue (500 nm) and violet (450 nm) wavelength bands demonstrating the strongest response to glucose variation. The integration of texture and spectral information enables a more comprehensive evaluation than using either modality alone, thereby improving the reliability of post-harvest grape quality assessment. Overall, the proposed multimodal approach provides a rapid, non-destructive, and cost-effective solution for intelligent grape sorting and has strong potential for implementation in smart post-harvest inspection systems. Future work will focus on expanding the dataset, validating the system using laboratory-based pesticide residue measurements, and integrating

advanced machine learning or deep learning algorithms to further improve classification performance.

REFERENCES

[1] Y. S. Parameswara and S. Susanto, "Perbaikan Teknik Pembrongsongan melalui Aplikasi Pestisida untuk Meningkatkan Kemulusan Buah Jambu Kristal (Psidium guajava L)," *Bul. Agrohorti*, vol. 7, no. 1, pp. 62–68, Jan. 2019.

[2] M. M. Pitoi, H. Harmoko, A. Tresnawati, H. F. Pardede, M. Ariyani, Y. S. Ridwan, and R. Yusiasih, "Pesticide residues in fruits and vegetables in Indonesia: Findings of five-year proficiency testing," *Accredit. Qual. Assur.*, vol. 27, no. 5, pp. 373–383, Oct. 2022.

[3] R. F. Suparman and A. Athennia, "Cemaran Bakteri dan Residu Pestisida Pada Buah Anggur," *J. Ilmiah Kesehatan*, vol. 11, no. 2, pp. 140–148, 2019.

[4] CNN Indonesia, "Fakta-fakta Geger Residu Zat Berbahaya Anggur Muscat di Thailand," *CNN Indonesia*, Oct. 29, 2024. [Online]. Available: https://www.cnnindonesia.com/internasional/20241029201031-106-1160965/fakta-fakta-geger-residu-zat-berbahaya-anggur-muscat-di-thailand

[5] Agritech, "Pasca Panen Anggur." [Online]. Available: http://agritech.50webs.com/Pasca%20Panen%20Anggur.html

[6] Government of Indonesia, *Peraturan Pemerintah Republik Indonesia Nomor 28 Tahun 2004 tentang Keamanan, Mutu, dan Gizi Pangan*. Jakarta, Indonesia: Sekretariat Negara, 2004.

[7] Badan Standardisasi Nasional (BSN), *Batas Maksimum Residu Pestisida pada Komoditas*. Jakarta, Indonesia: BSN, 2024.

[8] E. Ropelewska and Y. Noutfia, "Application of image analysis and machine learning for the assessment of grape (Vitis L.) berry behavior under different storage conditions," *European Food Research and Technology*, vol. 250, no. 3, pp. 935–944, 2024.

[9] V. Bhole, A. Kumar, and D. Bhatnagar, "A texture-based analysis and classification of fruits using digital and thermal images," in *ICT Analysis and Applications: Proceedings of ICT4SD 2019*, vol. 2. Singapore: Springer, 2020, pp. 333–343.

[10] R. Widodo, A. W. Widodo, and A. Supriyanto, "Pemanfaatan Ciri Gray Level Co-Occurrence Matrix (GLCM) Citra Buah Jeruk Keprok (Citrus reticulata Blanco) untuk Klasifikasi Mutu," *J. Pengembangan Teknol. Inf. dan Ilmu Komput.*, vol. 2, no. 11, pp. 5769–5776, 2018.

[11] C. C. Fagan et al., "Application of image texture analysis for online determination of curd moisture and whey solids in a laboratory-scale stirred cheese vat," *J. Food Sci.*, vol. 73, no. 6, pp. E250–E258, 2008.

[12] A. Afriadi, J. Harnaranda, and A. Ramadhanu, "Identifikasi Varietas Anggur Secara Otomatis Menggunakan Segmentasi Gambar Berbasis Warna dan Analisis Tekstur: Pendekatan K-Means Clustering," *KESATRIA: J. Penerapan Sistem Informasi (Manajemen & Komputer)*, vol. 5, no. 4, pp. 1973–1980, Oct. 2024.

[13] S. B. Sulistyo et al., "Portable Near Infrared Spectrometer dengan Sensor AS7263 untuk Pendugaan Sifat Kimia Jeruk Siam," *J. Teknol. Pertanian*, vol. 22, no. 2, pp. 81–88, Aug. 2021.

[14] U. Tamizheezham, I. Muthuvel, and A. Subbiah, "Effect of temperature on shelf life of Muscat Hamburg grapes under storage," *Madras Agricultural Journal*, vol. 105, pp. 286–290,2018.

[15] L. Cornehl, M. Schmidt, F. Meyer, M. Knauer, and T. Bocklitz, "Determination of sugars and acids in grape must using miniaturized near-infrared spectroscopy," *Sensors*, vol. 23, no. 11, Art. no. 5287, 2023.

[16] F. A. Fiddin, A. Rasyid, et al., "Designing Image Processing Based Banknote Identification Device for Blind People Using Raspberry Pi," Journal of Telecommunication Network (JARTEL), vol. 14, no. 1, pp. 84–91, 2024.

[17] F. B. Setiawan, O. J. A. Wijaya, L. H. Pratomo, and S. Riyadi, "Sistem Navigasi Automated Guided Vehicle Berbasis Computer Vision dan Implementasi pada Raspberry Pi," Jurnal Rekayasa Elektrika, vol. 17, no. 1, pp. 7–14, 2021.